Received: 10 November 2017 | Revised: 21 May 2018 | Accepted: 12 June 2018

DOI: 10.1002/dac.3768

RESEARCH ARTICLE

WILEY

Pilot contamination mitigation based on antenna subset transmission for mmWave massive MIMO

Nessrine Smaili[1] | Mustapha Djeddou[2] | Arab Azrar[1]

[1]Institut de Génie Electrique et Electronique ex-INELEC, Boulevard de l'indépendance 35000, Boumerdes, Algeria

[2]Communication Systems Laboratory, Military Polytechnic School, Algiers, Algeria

Correspondence
Mustapha Djeddou, EMP, BP 17, Bordj El Bahri, 16046, Algiers, Algeria. Present Address EMP, BP 17, Bordj El Bahri, 16046, Algiers, Algeria.
Email: djeddou.mustapha@gmail.com

Summary

This paper tackles the problem of pilot contamination (PC) in mmWave Massive MIMO cellular systems. We propose an analog precoder based on antenna subset transmission technique to mitigate the PC. This technique ensures the interfering signal to become noise-like signal thus helping a more efficient estimation of channel coefficients. Also, this strategy is low cost and introduces no complexity load. The result shows the effectiveness of the proposed precoder to mitigate PC issue.

KEYWORDS

antenna set transmission, massive MIMO, millimeter wave, pilot contamination

1 | INTRODUCTION

The fifth generation completes wireless communication with almost no limitation. Its goals include improving spectral efficiency and services, lowering cost and making uses of new spectrum. To meet these needs, many approaches are active research areas. Among these techniques, we cite millimeter Wave, small cell densification, and massive MIMO paradigm.[1] While the first approach pushes towards getting more spectrum by working in the nonexploited millimeter bands, the second one relies on network densification by integrating small to femtocells thus deploying more infrastructure to get more active users per area. The third approach involves the incorporation of a considerable number of antennas at the transmit and receive sides with the associated signal processing. Designing channel estimation (CE) based on pilot sequence with exploiting the sparsity of the channel is an important issue for mmWave Massive MIMO. Prior work has focused on hybrid beamforming design for multiuser channels and does not tackle the inter-cell interference problem.[2] However, Inter-cell interference in mmWave systems may be less severe due to signal blockage by urban objects. Furthermore, as next-generation networks are expected to have ultra-dense small cells, the dramatic shortening of inter-cell distances will reduce the blockage density in channels, resulting in sparse or even line-of-sight (LoS) interference channels. Hence, this problem becomes more critical in the presence of pilot contamination (PC). It is shown that channel estimation in massive MIMO multi-cell system hampered by the pilot contamination effect, constitutes a major bottleneck for overall performance.[3] This problem is a famous challenging issue that channel estimation suffer from. PC is defined by re-using the same band of frequencies with different factors among the cells. Moreover, the same orthogonal pilot sequences are re-used possibly and multiplied by an orthogonal transformation among the cells. Hence, the base station coherently combines signals from terminals in other cells. Recently, pilot contamination issue has attracted a great attention from the research community.[4,5] Indeed, Marzetta in Jose et al[5] pointed out the presence of this phenomenon which was not encountered in the single-cell scenario. There are several strategies proposed in the literature to overcome the pilot contamination issue. The main historical milestones of PC problem based on some pioneering papers are described in the literature.[4-7] Jose et al[5] analyze the PC problem with setting one user per cell and matched-filter (MF) precoding. Furthermore, they develop a new multi-cell MMSE-based precoding method that mitigates this problem. Zhang et al[8] have

proposed a channel estimation strategy which can mitigate PC without the knowledge of any side-information. There are several studies on suppressing inter-cell interference in multi-cell Massive MIMO mmWave systems. For instance, authors in Zhu et al[9] proved that the inter-cell interference level diminishes inversely with the array size, the square root of pilot sequence length and the spatial separation between paths, suggesting different ways of tackling pilot contamination. Where the paper[10] presents a direction of arrival (DOA) estimation using an estimation of the signal parameter via rotational invariance technique. Furthermore, Raza et al[11] study the impact of pilot contamination in mmWave and UHF-based Massive MIMO systems, considering a regular hexagonal geometry with a random deployment of users.

Wireless Massive MIMO mmWave communication systems offer many opportunities for 5G such as achieving significant higher spectral efficiency than conventional single-antenna systems.[12-14] But this performance gain comes at the cost of signal processing complexity increase at the receiver to counter-act the multi-user interference (MUI) in the presence of pilot contamination, that is emanated from the simultaneous data streams receptions from different users.

Many of the proposed techniques, cited above, to deal with PC issue introduce a high complexity load or suppose a cooperation between BS. In this paper, we address the problem of PC that beamforming can suffer due to the sidelobe signals.[5] The main contribution lies in the innovative systematic design of the analog beamformer precoder based on antenna subset transmission (AST) in mmWave massive MIMO cellular system. The AST has been proposed in Valliappan et al[15] that is based on randomizing the sidelobe′ patterns. Herein, the main idea of incorporating the AST is to cancel out the interfering signals by randomization in contaminated direction and keeping intact the transmission via the main lobe. Afterward, the standard channel estimation algorithms can then be applied. Also, the proposed approach exploits all transmit antennas. As result, the design respect mmWave hardware constraints.

2 | DATA MODEL AND PILOT CONTAMINATION PROBLEM

Consider an mmWave MIMO system composed of M_t and M_r transmit and receive antennas, respectively. We consider that both the transmitter and receiver are equipped with a limited number of radio frequency (RF) chains. To estimate the channel matrix, the transmitter sends a pilot signal $\mathbf{s}$, with unit energy, ($\|\mathbf{s}\|_2 = 1$) to the receiver. We consider the hybrid beamforming architecture, which combines $M_r \times N_{RF}$ analog beamformer, denoted by $\mathbf{F}$, N_{RF} RF chains, and $N_{RF} \times M_t$ digital beamformer, denoted by $\mathbf{W}$, with $\|\mathbf{F}\|_2 = \|\mathbf{W}\|_2 = 1$, respectively. The conventional estimator suffers from a lack of orthogonality between the desired and interfering pilots, an effect known as pilot contamination. In particular, when the same pilot sequence is reused in all L cells, ie, $\mathbf{s}_1 = \cdots = \mathbf{s}_L = \mathbf{s}$.

Without loss of generality, we consider a system with 2 cells and each with one user as the other users have orthogonal pilot sequences within the same considered cell. As shown in Figure 1, each user streams toward his BS via the main lobe, and signals from side-lobes reach the nearby BS. To transmit a signal, the BS applies 2 consecutive precoding operations $\mathbf{F} = \mathbf{F}_{BB}\mathbf{F}_{RF}$, where $\mathbf{F}_{BB}$ is the $N_{RF} \times Ns$ digital precoding performed in the base band and $\mathbf{F}_{RF}$ with a dimension of $M \times N_{RF}$ denotes the analog precoder. The elements of $\mathbf{F}_{RF}$ are considered as constant modules which are implemented using analog phase shifters. At the receiver side, the combiner $\mathbf{W} = \mathbf{W}_{RF}\mathbf{W}_{BB}$, composed of an RF combiner $\mathbf{W}_{RF}$ and a digital one $\mathbf{W}_{BB}$, is used to extract the transmitted data from the received signal. After different signal processing operations, the received signal at l^{th} BS is the following:

$$\mathbf{y} = \mathbf{w}^H(\sqrt{P_j}\mathbf{h}_{lj}(\theta, \alpha, \phi)\mathbf{f}_j\mathbf{s}_j + \sqrt{P_i}\mathbf{h}_{li}(\theta, \alpha, \phi)\mathbf{f}_i\mathbf{s}_i + \mathbf{n}), \tag{1}$$

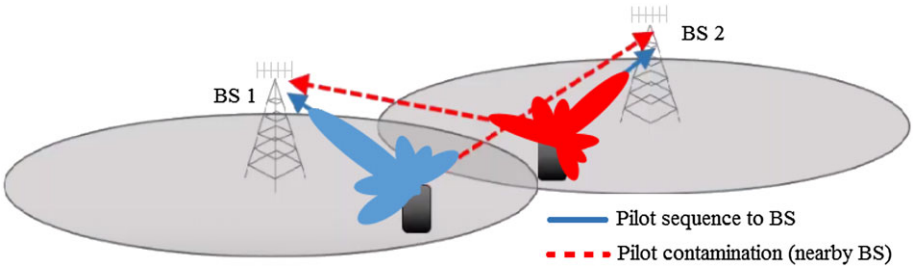

FIGURE 1 Illustration of the pilot contamination problem

where $(.)^H$ stands for the Hermitian. The indices j and i refer to the desired and interfering user of the l^{th} BS, respectively. P_j and P_i are the transmitted power of the desired and interfering user, respectively. The complex additive white Gaussian noise (AWGN) component is denoted by $\mathbf{n}$ with $\mathbf{n} \sim \mathcal{N}(0, \sigma_n^2)$. We adopt a geometric channel model along with a uniform linear array for simplicity of mathematical derivation but the proposed technique can be extended to any other antenna array configuration. The geometric channel model $\mathbf{h}(\theta, \alpha, \phi)$ is given by

$$\mathbf{h} = \sqrt{\frac{M_t M_r}{L}} \sum_{j=1}^{L} \alpha_j \mathbf{a}_{Rx}(\theta_{lj}) \mathbf{a}_{Tx}^*(\phi_{lj}), \tag{2}$$

where $(.)^*$ stands for the conjugate operator. $\mathbf{a}_{Rx}$ and $\mathbf{a}_{Tx}$ denote the reception and transmission antenna array manifold, respectively. Since the array is located along the x-y plane, the receiver's location is specified by the azimuth angle of arrival/departure. Therefore, θ_{lj} and ϕ_{lj} are the angles of arrival (AOA) and departure (AoD) between the user and the l^{th} BS respectively. The path loss gain is denoted by α_j. The received signal in (1) can be rewritten as follows:

$$\mathbf{y} = \mathbf{w}^H(\sqrt{P_j}\alpha_j \mathbf{h}_{lj}(\theta, \phi)\mathbf{f}_l \mathbf{s}_l + \sqrt{P_i}\alpha_i \mathbf{h}_{li}(\theta, \phi)\mathbf{f}_i \mathbf{s}_i + \mathbf{n}). \tag{3}$$

For simplicity, the receiver and transmitter beams are assumed to be aligned for maximum reception, ie, $\mathbf{w} = \mathbf{a}_r(\phi)$. This assumption is related to beam alignment problem, the reader may see Maschietti et al[16] and Hashemi et al[17] for more details about this issue. Replacing $\mathbf{w}$ in (3), we get the following:

$$\begin{aligned} \mathbf{y} &= \sqrt{P_j}\alpha_j \mathbf{a}_r^*(\phi)\mathbf{h}_{lj}(\theta, \phi)\mathbf{f}_l \mathbf{s}_l + \sqrt{P_i}\alpha_i \mathbf{a}_r^*(\phi)\mathbf{h}_{li}(\theta, \phi)\mathbf{f}_i \mathbf{s}_i + \mathbf{v} \\ &= \left(\sqrt{P_j}\alpha_j \mathbf{h}_{lj}(\theta)\mathbf{f}_l + \sqrt{P_i}\alpha_i \mathbf{h}_{li}(\theta)_{li}\mathbf{f}_i\right)\mathbf{s} + \mathbf{v}, \end{aligned} \tag{4}$$

where the modified noise component is denoted by $\mathbf{v} = \mathbf{w}^H(\phi)\mathbf{n}$.

2.1 | Proposed solution strategy

If we use directly the equation 4 to estimate the channel coefficients, the second term in the equation will make the estimation doubtful. Especially if we assume a perfect synchronization between the desired user and the interfering one which is the worst case in PC scenario.

In this section, we give details about the proposed solution. We incorporate AST to tackles the PC problem in mmWave Massive MIMO cellular system. Indeed, a new precoder design $\mathbf{F}$ is proposed based on AST. Instead of using all antennas for beamforming, a set of random antennas are used for coherent beamforming, whereas the remaining antennas are set to combine destructively. The indices of these antennas are randomized in every symbol transmission. This randomizes the beam pattern sidelobes and as a result, produces noise-like signals at nondesired directions. Indeed, the BS would observe a fixed gain reduction (due to destructive combining) and a noise-like interference coming from the contaminating user. As mentioned, we adopt a uniform linear array (ULA) with isotopic antennas along the x-axis and the array centered at the mid of the array. Even so, the proposed technique can be adapted to any arbitrary antenna structures. Let $I_{M_{sub}}(k)$ be the random subset of M_{sub} out of M_t antennas used to transmit the k^{th} symbol, $I_{L_t}(k)$ be a subset that contains the indices of the remaining antennas. The precoder design is a function of symbol index k, so with every symbol, a new precoder is used with a different beam pattern. Indeed, we are changing the phase θ randomly in the interval $(0, 2\pi)$. Hence, θ is uniformly distributed. To obtain the randomization, we use a Walsh sequence generator. Walsh Codes are a set of orthonormal codes. Therefore, the generated Walsh sequences C contains an equal number of 1's and -1's but they are randomly distributed from one shot to another. Walsh is closed in a standard interval $(0, 1)$ and every function takes the values $+1, -1$ except the final number, which is zero.[18] The resulted antenna phase shifts are the following:

$$\Psi_n(k) = \begin{cases} \Upsilon_n(k) & n \in I_{M_{sub}}(k) \\ \Upsilon_n(k) * C, & n \in I_{L_t}(k), \end{cases} \tag{5}$$

where $(*)$ stands for element-wise multiplication and $\Upsilon_n(k) = (\frac{M_t - 1}{2} - n)2\pi\frac{d}{\lambda}cos(\theta_{lj})$ is a phase shift valid for the adopted antenna array configuration (ULA). Therefore, the transmitter precoder defined by

$$\mathbf{f}(k) = \frac{1}{\sqrt{M_t}} e^{j\Psi(k)}. \tag{6}$$

An example of random selection of uniform linear array ULA is illustrated in Figure 2. For every pilot symbol, a set of antennas are settled to combine coherently (black color) whereas the other remaining antennas (black and red antennas) are set to combine destructively. After choosing randomly the M_{sub} antennas for the main beam pattern (black antennas), one of the random Walch sequences is set to the black and red antennas. For example, for C= [1 −1 −1 −1 1 1 −1 1] will give us the configuration in figure 2 where 1's are set for antennas in red and −1s for black antennas. This configuration is altered at every new pilot symbol. For example, the first "black antenna" can become a red or a black one and so is for other antennas.

Another example concerning the obtained antenna beam pattern is depicted in Figure 3. In this figure, we plot the beam-pattern versus the transmitted angle using 32 and 16 transmit antennas. In Figure 3, the randomness of antenna selection only appears in the region of side lobes, and there is no randomness in the region of the main lobe. Also, it is shown that the beam-pattern of the proposed technique varies at all angular locations except at the transmitted angular

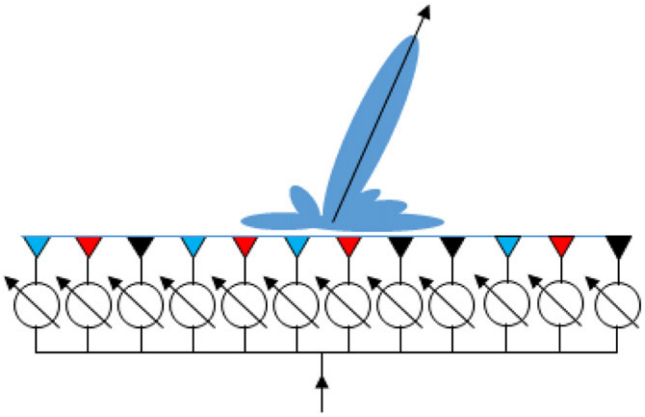

FIGURE 2 Antenna selection pattern for a uniform linear array: black antennas coherently co-phased to combine at BS, black and red antennas co-phased to destructively combine at BS

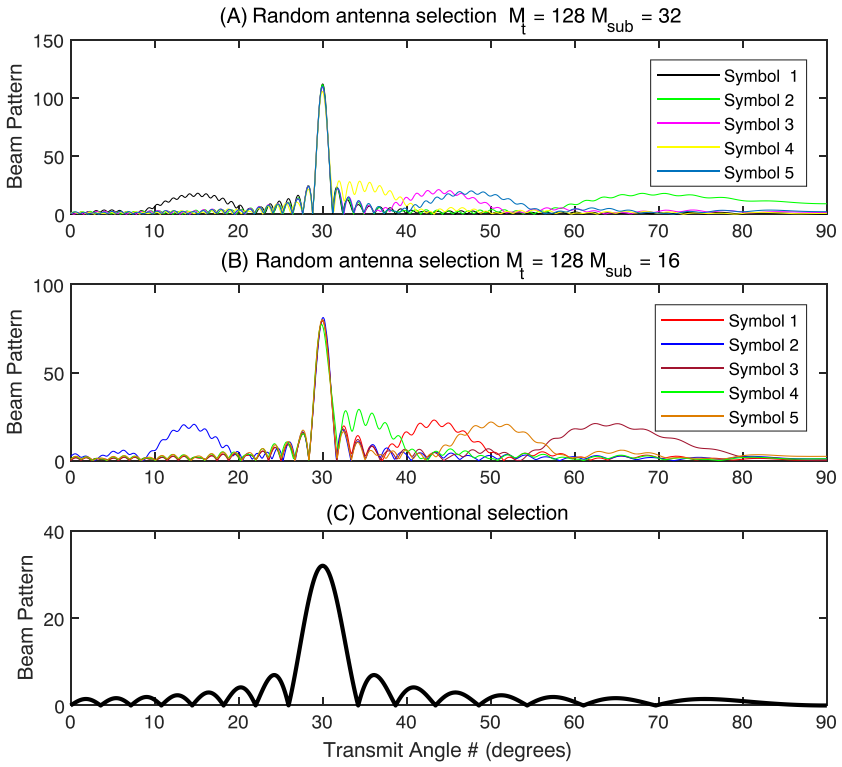

FIGURE 3 Successive antenna beam patterns using randomization (A & B) and conventional radiation (C)

location ($\theta = 30°$ in this example). While the conventional array transmission techniques result in a constant radiation pattern at contaminated user, ie, large sidelobes on average and a unique beam pattern along all the emitted symbols.

To show the contribution of the used approach, the data models obtained for the 2 cases, conventional and AST transmissions, are to be considered.

2.1.1 | Conventional array transmission

In conventional array transmission, the transmitter precoder defined in (6) is placed in the equation 4, we get the following:

$$\begin{aligned}\mathbf{y} &= \sqrt{\frac{P_j M_r}{M_t}}\alpha_j \sum_{n=0}^{M_t-1} e^{j(n-\frac{M_t-1}{2})\frac{2\pi d}{\lambda}(cos\theta_{lj}-cos\theta_{lj})}\mathbf{s} + \sqrt{\frac{P_i M_r}{M_t}}\alpha_i \sum_{n=0}^{M_t-1} e^{j(n-\frac{M_t-1}{2})\frac{2\pi d}{\lambda}(cos\theta_{lj}-cos\theta_{li})}\mathbf{s} + \mathbf{v} \\ &= \sqrt{P_j M_r M_t}\alpha_j \mathbf{s} + \sqrt{\frac{P_i M_r}{M_t}}\alpha_i \left(e^{-j\frac{M_t-1}{2}\frac{2\pi d}{\lambda}(cos\theta_{lj}-cos\theta_{li})} \sum_{n=0}^{M_t-1} e^{jn\frac{2\pi d}{\lambda}(cos\theta_{lj}-cos\theta_{li})} \right)\mathbf{s} + \mathbf{v},\end{aligned} \tag{7}$$

where the angles θ_{lj} and θ_{li} are the AOAs of mainlobe and sidelobes of users signals j and i, respectively. The angle θ_{li} belongs to the contaminating user. Whereas θ_{lj} behooves to the desired user.

The summation in the second term of (7) is an exponential sum of the form $\sum_{k=0}^{N-1} r^k = \frac{1-r^N}{1-r}$. Hence, we get the following:

$$\begin{aligned}\mathbf{y} &= \sqrt{P_j M_r M_t}\alpha_j \mathbf{s} + \sqrt{\frac{P_i M_r}{M_t}}\alpha_i \left[e^{-j(\frac{M_t-1}{2})2\pi\frac{d}{\lambda}(cos\theta_{lj}-cos\theta_{li})} \left(\frac{1-e^{jM_t 2\pi\frac{d}{\lambda}(cos\theta_{lj}-cos\theta_{li})}}{1-e^{j2\pi\frac{d}{\lambda}(cos\theta_{lj}-cos\theta_{li})}} \right) \right] \\ &= \sqrt{P_j M_r M_t}\alpha_j \mathbf{s} + \sqrt{\frac{P_i M_r}{M_t}}\alpha_i \left(\frac{sinM_t\frac{\pi d}{\lambda}(cos\theta_{lj}-cos\theta_{li})}{sin\frac{\pi d}{\lambda}(cos\theta_{lj}-cos\theta_{li})} \right)\mathbf{s} + \mathbf{v}.\end{aligned} \tag{8}$$

2.1.2 | Antenna subset transmission

In Antenna subset transmission (AST), the entries of the transmitting beamformer vector $\mathbf{f}(k)$ are placed in (5). Hence, the received signal in (4) becomes

$$\begin{aligned}\mathbf{y} = &\sqrt{\frac{P_j M_r}{M_t}}\alpha_j \left[\sum_{m\in I_{M_{sub}}(k)} e^{-j(\frac{M_t-1}{2}-m)\frac{2\pi d}{\lambda}cos\theta_{lj}} e^{j(\frac{M_t-1}{2}-m)\frac{2\pi d}{\lambda}cos\theta_{lj}} \right. \\ &+ \sum_{n\in I_{L_t}(k)} e^{-j(\frac{M_t-1}{2}-n)\frac{2\pi d}{\lambda}cos\theta_{lj}} e^{j(\frac{M_t-1}{2}-n)\frac{2\pi d}{\lambda}cos\theta_{lj}} - \left. \sum_{n\in I_{L_t}(k)} e^{-j(\frac{M_t-1}{2}-n)\frac{2\pi d}{\lambda}cos\theta_{lj}} e^{j(\frac{M_t-1}{2}-n)\frac{2\pi d}{\lambda}cos\theta_{lj}} \right]\mathbf{s} \\ &+ \sqrt{\frac{P_i M_r}{M_t}}\alpha_i \left[\sum_{m\in I_{M_{sub}}(k)} e^{-j(\frac{M_t-1}{2}-m)\frac{2\pi d}{\lambda}cos\theta_{lj}} e^{j(\frac{M_t-1}{2}-m)\frac{2\pi d}{\lambda}cos\theta_{li}} + \sum_{n\in I_{L_t}(k)} e^{-j(\frac{M_t-1}{2}-n)\frac{2\pi d}{\lambda}cos\theta_{lj}} e^{j(\frac{M_t-1}{2}-n)\frac{2\pi d}{\lambda}cos\theta_{li}} \right. \\ &- \left. \sum_{n\in I_{L_t}(k)} e^{-j(\frac{M_t-1}{2}-n)\frac{2\pi d}{\lambda}cos\theta_{lj}} e^{j(\frac{M_t-1}{2}-n)\frac{2\pi d}{\lambda}cos\theta_{li}} \right]\mathbf{s} + \mathbf{v} \\ = &\sqrt{\frac{P_j M_r}{M_t}}\alpha_j \left[\sum_{m\in I_{M_{sub}}(k)} e^{-j(\frac{M_t-1}{2}-m)\frac{2\pi d}{\lambda}(cos\theta_{lj}-cos\theta_{lj})} + \sum_{m\in I_{L_t}(k)} e^{-j(\frac{M_t-1}{2}-n)\frac{2\pi d}{\lambda}(cos\theta_{lj}-cos\theta_{lj})} \right. \\ &- \left. \sum_{n\in I_{L_t}(k)} e^{-j(\frac{M_t-1}{2}-n)\frac{2\pi d}{\lambda}(cos\theta_{lj}-cos\theta_{lj})} \right]\mathbf{s} + \sqrt{\frac{P_i M_r}{M_t}}\alpha_i \left[\sum_{m\in I_{M_{sub}}(k)} e^{-j(\frac{M_t-1}{2}-m)\frac{2\pi d}{\lambda}(cos\theta_{lj}-cos\theta_{li})} \right. \\ &+ \left. \sum_{n\in I_{L_t}(k)} e^{-j(\frac{M_t-1}{2}-n)\frac{2\pi d}{\lambda}(cos\theta_{lj}-cos\theta_{li})} - \sum_{n\in I_{L_t}(k)} e^{-j(\frac{M_t-1}{2}-n)\frac{2\pi d}{\lambda}(cos\theta_{lj}-cos\theta_{li})} \right]\mathbf{s} + \mathbf{v} = \left(\sqrt{\frac{P_j M_r}{M_t}}\alpha_j M_{sub} + \sqrt{P_i M_r}\alpha_i \boldsymbol{\beta} \right)\mathbf{s} + \mathbf{v}.\end{aligned} \tag{9}$$

The term $\boldsymbol{\beta}$ in (9) is

$$\boldsymbol{\beta} = \sqrt{\frac{1}{M_t}}\left(\sum_{m \in I_{M_{sub}}(k)} e^{-j(\frac{M_t-1}{2}-m)\frac{2\pi d}{\lambda}(cos\theta_{lj}-cos\theta_{li})} + \sum_{n \in I_{L_t}(k)} e^{-j(\frac{M_t-1}{2}-n)\frac{2\pi d}{\lambda}(cos\theta_{lj}-cos\theta_{li})} - \sum_{n \in I_{L_t}(k)} e^{-j(\frac{M_t-1}{2}-n)\frac{2\pi d}{\lambda}(cos\theta_{lj}-cos\theta_{li})} \right). \tag{10}$$

Since the entries of $I_{M_{sub}}(k)$ and $I_{L_t}(k)$ are randomly selected for each data symbol, (10) can be simplified to

$$\boldsymbol{\beta} = \sqrt{\frac{1}{M_t}} \sum_{m=0}^{M_t-1} B_m e^{-j(\frac{M_t-1}{2}-m)\frac{2\pi d}{\lambda}(cos\theta_{lj}-cos\theta_{li})}. \tag{11}$$

In AST, the selected number of antenna M_{sub} are chosen independently at random from M_t for each symbol; therefore, by definition, we adopt an independent Bernoulli random variable. Indeed, the well know distribution is characterized by its parameters p and q. By denoting B_m as the Bernoulli random variable so, when $B_m = 1$ the probability is $p = \frac{(M_{sub}+\frac{M_t-M_{sub}}{2})}{M_t} = \frac{M_t+M_{sub}}{2M_t}$ whereas, for $B_m = -1$ the probability is $q = \frac{M_t-M_{sub}}{2M_t}$.[15] We note that if $\theta_{li} = \theta_{lj}$, $\boldsymbol{\beta}$ will be a constant, the random behavior is obtained when $\theta_{li} \neq \theta_{lj}$, thus the destructive combination is obtained in the last case. As $\boldsymbol{\beta}$ is a random variable, we need to evaluate its statistical characteristics. For a large number of antennas M_t, $\boldsymbol{\beta}$ is a summation of distributions. Referring to central limits theorem, $\boldsymbol{\beta}$ is a Gaussian random variable that is completely characterized by its mean and variance.

(a) **Mean of$\boldsymbol{\beta}$**:

$$E(\boldsymbol{\beta}) = \sqrt{\frac{1}{M_t}} \sum_{m=0}^{M_t-1} E(B_m) e^{-j(\frac{M_t-1}{2}-m)\frac{2\pi d}{\lambda}(cos\theta_{lj}-cos\theta_{li})}, \tag{12}$$

where E is the mathematical expectation, with

$$\begin{aligned} E(B_m) &= p \times (1) + q \times (-1) \\ &= \frac{M_t + M_{sub}}{2M_t} - \frac{M_t - M_{sub}}{2M_t} = \frac{M_{sub}}{M_t}. \end{aligned} \tag{13}$$

Equation (12) can be rewritten as follows:

$$E(\boldsymbol{\beta}) = \frac{M_{sub}}{M_t} \sqrt{\frac{1}{M_t}} \sum_{m=0}^{M_t-1} e^{-j(\frac{M_t-1}{2}-m)\frac{2\pi d}{\lambda}(cos\theta_{lj}-cos\theta_{li})}. \tag{14}$$

Using the same steps in (7) and (8), we obtain the following:

$$E(\boldsymbol{\beta}) = \frac{M_{sub}}{M_t} \sqrt{\frac{1}{M_t}} \left(\frac{sinM_t \frac{\pi d}{\lambda}(cos\theta_{lj} - cos\theta_{li})}{sin\frac{\pi d}{\lambda}(cos\theta_{lj} - cos\theta_{li})} \right). \tag{15}$$

(b) **Variance of$\boldsymbol{\beta}$**:

$$\mathrm{Var}(\boldsymbol{\beta}) = \frac{1}{M_t} \sum_{m=0}^{M_t-1} \mathrm{Var}(B_m) e^{-j2(\frac{M_t-1}{2}-m)\frac{2\pi d}{\lambda}(cos\theta_{lj}-cos\theta_{li})}, \tag{16}$$

where

$$\mathrm{Var}(B_m) = E(B_m^2) - (E(B_m))^2. \tag{17}$$

We calculate the first term of (17) as follows:

$$E(B_m^2) = p(1)^2 + q(-1)^2 = \frac{M_t + M_{sub}}{2M_t}(1) + \frac{M_t - M_{sub}}{2M_t}(1) = 1. \tag{18}$$

Hence, we obtain the variance:

$$\mathrm{Var}(B_m) = 1 - \frac{M_{sub}^2}{M_t^2}. \tag{19}$$

Finally, the variance in (16) can be expressed as follows:

$$\begin{aligned}\mathrm{Var}(\boldsymbol{\beta}) &= \frac{M_t^2 - M_{sub}^2}{M_t^3} \sum_{m=0}^{M_t-1} e^{-j2(\frac{M_t-1}{2}-m)\frac{2\pi d}{\lambda}(cos\theta_{lj}-cos\theta_{li})} \\ &= \frac{M_t^2 - M_{sub}^2}{M_t^3} \left(\frac{sinM_t\frac{2\pi d}{\lambda}(cos\theta_{lj}-cos\theta_{li})}{sin\frac{2\pi d}{\lambda}(cos\theta_{lj}-cos\theta_{li})} \right).\end{aligned} \tag{20}$$

3 | SIGNAL TO INTERFERENCE RATIO DERIVATION

In this section, we derive the signal-to-interference ratio (SIR) for both 2 cases: antenna subset and conventional array transmissions.[6] The SIR formula is given as follows:

$$\mathbf{SIR} = \frac{\| \sqrt{P_j}\alpha_j \mathbf{a}_r^*(\phi)\mathbf{h}_{lj}\mathbf{f}_l \|^2}{\| \sqrt{P_i}\alpha_i \mathbf{a}_r^*(\phi)\mathbf{h}_{li}\mathbf{f}_i \|^2}. \tag{21}$$

1. Conventional array transmission: Using Equations 8 and 21, the obtained SIR is

$$\begin{aligned}\mathbf{SIR_{CAT}} &= \frac{\left(\sqrt{P_j M_r M_t}\alpha_j \right)^2}{\left(\sqrt{\frac{P_i M_r}{M_t}}\alpha_i \frac{sin(M_t\frac{\pi d}{\lambda}(cos\theta_{lj}-cos\theta_{li}))}{sin(\frac{\pi d}{\lambda}(cos\theta_{lj}-cos\theta_{li}))} \right)^2} \\ &= \frac{P_j M_t^2 \alpha_j^2}{P_i\alpha_i^2 \left(\frac{sin(M_t\frac{\pi d}{\lambda}(cos\theta_{lj}-cos\theta_{li}))}{sin(\frac{\pi d}{\lambda}(cos\theta_{lj}-cos\theta_{li}))} \right)^2}.\end{aligned} \tag{22}$$

2. AST selection: By using (9), the SIR presented in (21) becomes

$$\begin{aligned}\mathbf{SIR_{AST}} &= \frac{\frac{P_j M_r \alpha_j^2 M_{sub}^2}{M_t}}{P_i M_r \alpha_i^2 \mathrm{Var}(\boldsymbol{\beta})} \\ &= \frac{P_j \alpha_j^2 M_{sub}^2 M_t^2}{P_i\alpha_i^2 \left[(M_t^2 - M_{sub}^2) \left(\frac{sinM_t\frac{2\pi d}{\lambda}(cos\theta_{lj}-cos\theta_{li})}{sin\frac{2\pi d}{\lambda}(cos\theta_{lj}-cos\theta_{li})} \right) \right]}.\end{aligned} \tag{23}$$

Now, using some trigonometric identities, we express the following ratio:

$$\begin{aligned}Fa &= \frac{\mathbf{SIR_{AST}}}{\mathbf{SIR_{CAT}}} \\ &= \frac{M_{sub}^2}{(M_t^2 - M_{sub}^2)} \times \left(\frac{tan(M_t\frac{\pi d}{\lambda}(cos\theta_{lj}-cos\theta_{li}))}{tan(\frac{\pi d}{\lambda}(cos\theta_{lj}-cos\theta_{li}))} \right).\end{aligned} \tag{24}$$

In the above equation, we have assumed that the path losses α_i and α_j are equal and the signal power $P_i = P_i = 1$.

To determine the suitable number M_{sub} to have a factor greater than unity, we have represented the factor Fa, defined in 24, versus M_{sub} in Figure 4. According to the obtained curves, it follows that it is desirable to use M_{sub} as close as possible to M_t to have a factor Fa greater than unity. If M_{sub} is correctly settled, this will lead to $\mathbf{SIR_{AST}} > \mathbf{SIR_{CAT}}$.

Thereby, the key feature in the AST based PC mitigation is the choice of the number of antennas M_t and M_{sub}. In Figure 5, we sketch the *SIR* evolution versus the number of used antennas M_t in user side where M_{sub} is taken as a factor of M_t. The obtained results reveal that increasing M_t gives better performance while increasing the ratio $\frac{M_t}{M_{sub}}$ degrades

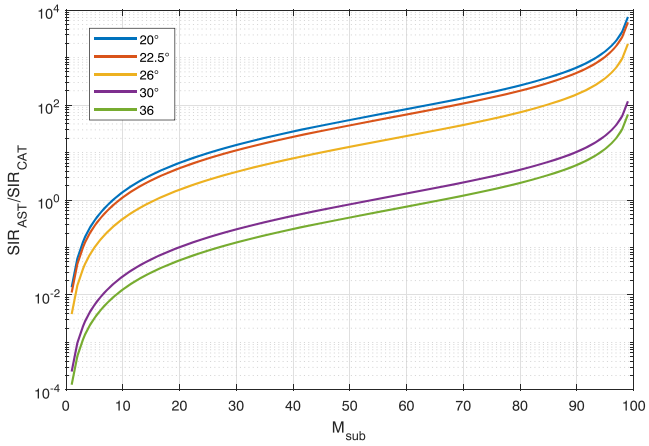

FIGURE 4 Ratio Fa versus M_{sub}, $M_t = 100$ and $\theta_i = 22°$

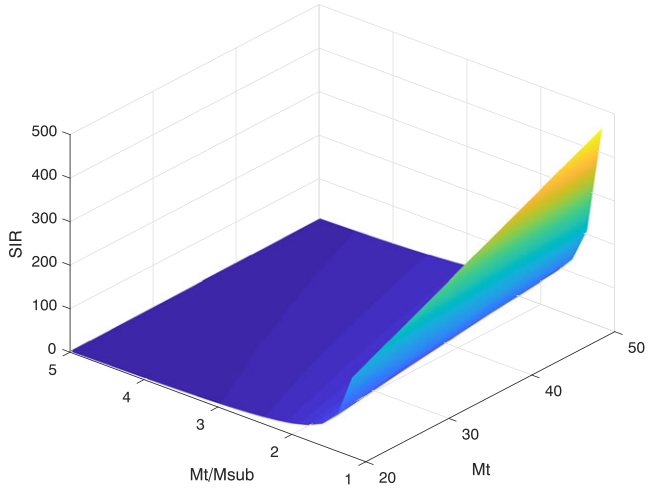

FIGURE 5 Signal to interference ratio (SIR) versus M_t and M_{sub}. $\theta_i = 70°$ and $\theta_j = 160°$

the performance for all cases. This is due to the fact that increasing the ratio, makes the main lobe much wider as fewer antennas are used for streaming the symbols thus the BS receive less power from the desired direction. Hence, the best interval for the ratio is [1.2, 2]. Also, this figure reveals that using less than the half of antennas for the mainlobe is not suitable as the performance degrades dramatically. Generally, using more antennas is beneficial and the only limit is the practical realization of such array, in some UE it is not possible to use a large number of antennas.

The designed precoder can be used at UE or BS level. The only requirement is the presence of an antenna array (this condition may be not satisfied in some microwave systems at UE level). Thus, it is not specific to the mmWave system but can be used in microwave system at least in the BS. After designing the AST-based precoder, a channel estimation algorithm can be used in presence of PC. Afterward, hybrid precoders/combiners, ($\mathbf{F}_{RF}, \mathbf{F}_{BB}, \mathbf{W}_{RF}, \mathbf{W}_{BB}$) are settled at both the BS and UE to maximize the data rate of transmission over the Massive MIMO mmWave systems (1). Hence, to confirm the effectiveness of the proposed approach, spectral efficiency (SE) is calculated at the user level. The equation of SE is defined as follows[19]:

$$\mathbf{Rate} = \log_2\left(\left|\mathbf{I}_{N_s} + \frac{\alpha}{N_s}\mathbf{R}_n^{-1}\mathbf{W}_{BB}^{*}\mathbf{W}_{RF}^{*}\mathbf{H}\mathbf{F}_{RF}\mathbf{F}_{BB} \times \mathbf{F}_{BB}^{*}\mathbf{F}_{RF}^{*}\mathbf{H}\mathbf{W}_{RF}\mathbf{W}_{BB}\right|\right), \tag{25}$$

where $\mathbf{R}_n^{-1} = \sigma_n^2\mathbf{W}_{BB}^{*}\mathbf{W}_{RF}^{*}\mathbf{F}_{RF}\mathbf{F}_{BB}$ denotes for the noise covariance matrix and σ_n^2 is the noise variance at UE level. The expression of the matrices $\mathbf{W}_{BB}^{*}, \mathbf{W}_{RF}^{*}, \mathbf{F}_{RF}, \mathbf{F}_{BB}$ depend on the used precoding techniques (purely digital, purely analog, or hybrid precoding).[2,9,20,21]

4 | PERFORMANCE EVALUATION

In this section, we consider 2 simulation configurations, we begin with 2 cells system each with one user sending the same pilot signals to BS of cell 1. The second configuration considers three cells configuration. Simulations are conducted for the proposed AST scheme along with the conventional transmission counterpart in the presence of PC. The simulation parameters are fixed and generated as the ones used in Alkhateeb et al[2] and we used the same channel estimation technique. Herein, the BS has $M_r = 64$ antennas, the AST technique is applied in the MS side, so M_r has not an impact on the AST performance. Certainly, increasing M_r will increase performance but this is due to MIMO gain rather than to AST technique; 10 RF chains are used with a transmitted power of 37 dBm. The mobile station (MS) uses 64, 128, and 256 antennas and 6 RF chains. Both the BS and the MS are equipped with uniform linear array (ULA) with an inter-element spacing of $\lambda/2$. The number of transmitted data streams is $N_s = 3$. Hybrid precoder concept divides the precoding operations into 2 cascaded stages, namely, the low-dimensional baseband precoding and the high dimensional phase-only processing at the RF domain. We use the geometric channel model with an average power gain of $P_R = 1$ and a single path. The AoAs/AoDs are assumed to be uniformly distributed between 0 and 2π. The system is assumed to operate at 28 GHz carrier frequency and has a band width of 100 MHz with path loss exponent $n_{pl} = 3$. Moreover, to examine the behavior of the SE, 4 scenarios are simulated. The first scenario is based on the perfect CSI knowledge along with unconstrained precoding and is used as a benchmark to other scenarios. Here, unconstrained precoding means that only digital beamforming (no analog precoding is in order) is used.[22] The second and the third scenario are constrained cases where we use an hybrid precoding but with and without pilot contamination. We expect that the proposed technique lies between these last two scenarios. In all the 3 scenarios, conventional transmission is used, only our proposal uses AST-based precoder with $M_{sub} = 32$.

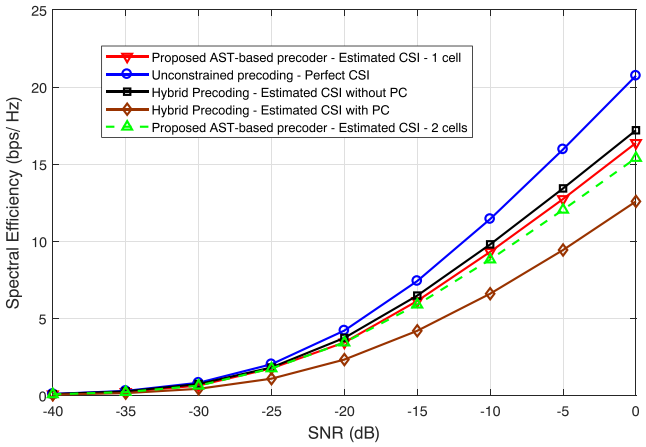

FIGURE 6 Spectral efficiency (SE) comparison with $M_t = 64$

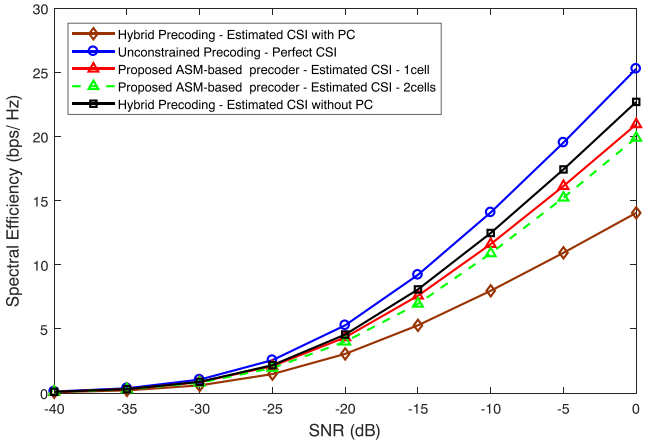

FIGURE 7 Spectral efficiency (SE) comparison with $M_t = 128$

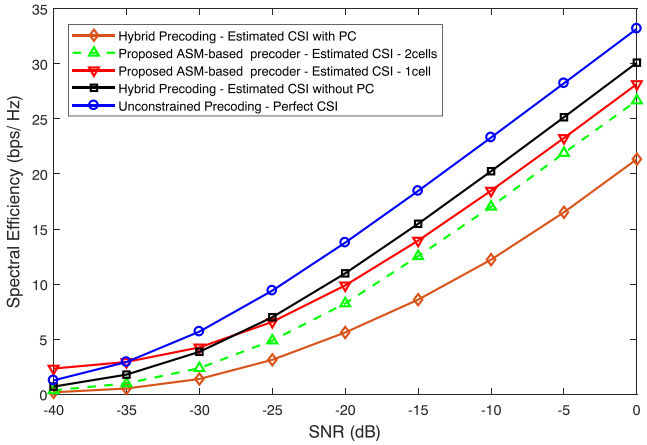

FIGURE 8 Spectral efficiency (SE) comparison with $M_t = 256$

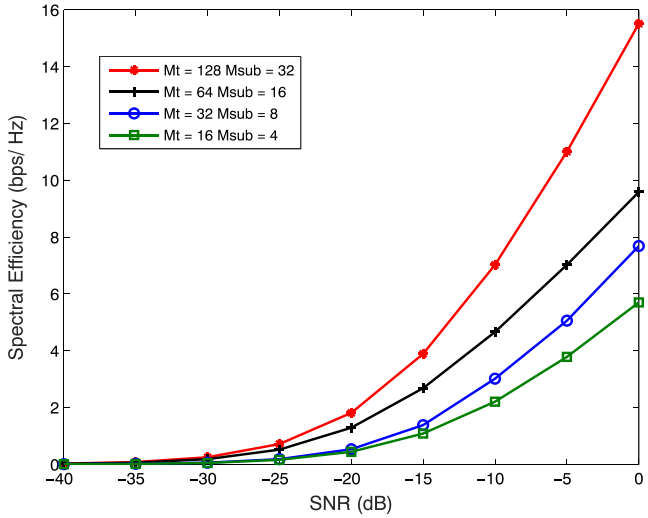

FIGURE 9 Spectral efficiency (SE) for different values of M_{sub} with a fixed ratio $M_t/M_{sub} = 4$

It appears from the results reported in Figure 6 that the application of the proposed AST in the presence of PC allows achieving better SE, as compared with conventional one. Whereas, the results indicate that comparable gains can be achieved using the proposed scheme with a perfect CSI. We can remark that at SNR of $-5dB$, the random selection has SE gain of $5bps/Hz$ compared to conventional selection. Also, we can see that the achieved SE in the presence of PC of the proposed scheme is very close to the case without PC. This results are confirmed in the Figures 7 and 8 where M_t is set to 128 and 256, respectively. The SE performance keeps increasing. Noting also that a slight difference occurs when we increase M_t and keeping M_{sub} fixed (comparing AST-based technique to the PC-free system), in fact, it confirms the results in (5) where it is suitable to keep a factor around 2 for better performance.

In the second part, we consider the configuration case of 3 cells (2 neighboring cells each with one contaminating UE), a slight decrease of SE (dashed green line curves in Figures 6, 7, and 8) is observed but our proposal still achieve good performance. Hence, we can deduce that the random antenna selection has better performance than the fixed antenna selection even in the presence of PC. This can be explained by the gain factor of (M_{sub}^2) that appear in (23), and reduction of the amount of contaminating user interference when comparing the 2 equations 22 and 23. Hence, The SIR improvements achieved by the proposed configuration provides a significant gain in SE.

To assess the performance of the proposed technique in term of used antennas for randomization, the spectral efficiency of the proposed antenna selection is compared for a different number M_t and M_{sub}, while keeping the same ratio, ie, $R = \frac{M_t}{M_{sub}} = 4$ for each curve. We assume the same simulation parameters with Figure 6 except for the number of antennas M_t. From Figure 9, it is observed that the spectral efficiency brought from $M_{sub} = 32$ is significant over $M_{sub} = 16$, $M_{sub} = 8$ and $M_{sub} = 4$. Thereby, increasing the number of random and total antenna, while fixing the ratio between them results

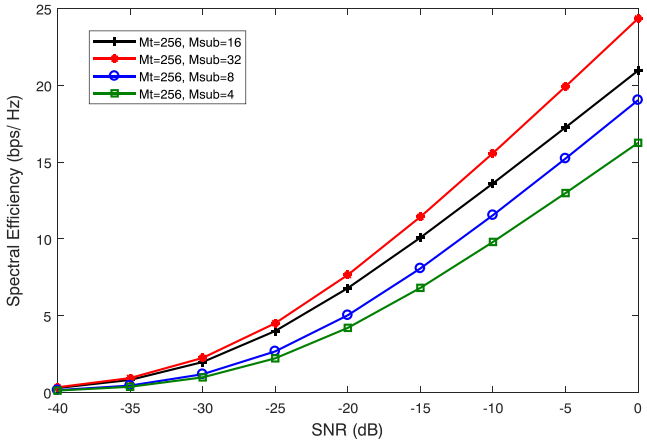

FIGURE 10 Spectral efficiency (SE) for different values of M_{sub} with a fixed value M_t

in improvement of the performance. This can be explained by the fact that increasing M_{sub} makes the sidelobes signals more noise-like and also keeping the ratio constant makes the main lobe more directive, hence more effective in directing the desired signal power to the desired BS. As a result, the number of selected random antenna arising from the proposed scheme in mmWave Massive MIMO has a drastic effect on the performance. Figure 10 depicts the SE performance while keeping M_t fixed and varying M_{sub}, the same remark can be made, increasing M_{sub} increase the performance, it is better to have M_{sub} close to M_t to maximize the performance.

5 | CONCLUSION

In this paper, we have proposed an approach to deal with PC issue in mmWave massive MIMO cellular system. The proposed precoder uses AST for mitigating the PC problem. Hence, the novelty of this work is based on distorting the sidelobes signal by generating a random sequence using Walsh codes and as result, it combines in a destructive manner in reception. To confirm our approach, simulation results indicate that the proposed precoder realizes SE gain that is close to the one of PC free system. Moreover, the adopted technique is of low cost as no hardware complexity is added compared with conventional systems.

ORCID

Mustapha Djeddou http://orcid.org/0000-0001-5840-118X

REFERENCES

1. Han S, Chih-Lin I, Xu Z, Rowell C. Large-scale antenna systems with hybrid analog and digital beamforming for millimeter wave 5g. *IEEE Commun Mag*. 2015;53(1):186-194.
2. Alkhateeb A, ElAyach O, Leus G, Heath RW. Channel estimation and hybrid precoding for millimeterwave cellular systems. *IEEE J Sel Top Sign Proces*. 2014;8(5):831-846.
3. Yin H, Gesbert D, Filippou M, Liu Y. A coordinated approach to channel estimation in large-scale multiple-antenna systems. *IEEE J Sel Areas Commun*. 2013;31(2):264-273.
4. Hoydis J, Ten Brink S, Debbah M. Massive MIMO: How many antennas do we need? In: Communication, Control, and Computing (Allerton), 2011 49th Annual Allerton Conference on. IEEE; 2011; Urbana-Champaign, IL, United States:545-550.
5. Jose J, Ashikhmin A, Marzetta TL, Vishwanath S. Pilot contamination and precoding in multi-cell TDD systems. *IEEE Trans Wirel Commun*. 2011;10(8):2640-2651.
6. Marzetta TL. Noncooperative cellular wireless with unlimited numbers of base station antennas. *IEEE Trans Wirel Commun*. 2010;9(11):3590-3600.
7. Elijah O, Leow CY, Rahman TA, Nunoo S, Iliya SZ. A comprehensive survey of pilot contamination in massive MIMO 5g system. *IEEE Commun Surv Tutorials*. 2016;18(2):905-923.
8. Zhang J, Zhang B, Chen S, Mu X, El-Hajjar M, Hanzo L. Pilot contamination elimination for large-scale multiple-antenna aided OFDM systems. *IEEE J Sel Top Sign Proces*. 2014;8(5):759-772.

9. Zhu G, Huang K, Lau VK, Xia B, Li X, Zhang Sha. Hybrid Beamforming via the Kronecker Decomposition for the Millimeter-Wave Massive MIMO Systems. arXiv preprint arXiv 1704.03611; 2017.
10. Rubayet S, Estimation LL. Performance Analysis for Multi-Cell Multi-User 3D mmWave Massive-MIMO OFDM System. In: Wireless Communications and Networking Conference (WCNC) 2017 IEEE. IEEE; 2017; San Francisco, CA, USA:1-6.
11. Raza NSA, Ali HS, Mulk Z. Pilot reuse and sum rate analysis of mmWave and UHF-based massive MIMO systems. In: Vehicular Technology Conference (VTC Spring), 2016 IEEE 83rd. IEEE; 2016; Nanjing, China:1-5.
12. Swindlehurst AL, Ayanoglu E, Heydari P, Capolino F. Millimeter-wave massive MIMO: the next wireless revolution?*IEEE Commun Mag*. 2014;52(9):56-62.
13. Sun S, Rappaport TS, Heath RW, Nix A, Rangan S. MIMO For millimeter-wave wireless communications: beamforming, spatial multiplexing, or both?*IEEE Commun Mag*. 2014;52(12):110-121.
14. Kulkarni MN, Ghosh A, Andrews JG. A comparison of MIMO techniques in downlink millimeter wave cellular networks with hybrid beamforming. *IEEE Trans Commun*. 2016;64(5):1952-1967.
15. Valliappan N, Lozano A, Heath RW. Antenna subset modulation for secure millimeter-wave wireless communication. *IEEE Trans Commun*. 2013;61(8):3231-3245.
16. Maschietti F, Gesbert D, Kerret P, Wymeersch H. Robust location-aided beam alignment in millimeter wave massive MIMO. arXiv preprint arXiv 1705.01002; 2017.
17. Hashemi M, Sabharwal A, Koksal CEmre, Shroff NB. ; 2017.
18. Walsh JL. A closed set of normal orthogonal functions. *Am J Math*. 1923;45(1):5-24.
19. Goldsmith A, Jafar SA, Jindal N, Vishwanath S. Capacity limits of MIMO channels. *IEEE J Sel Areas Commun*. 2003;21(5):684-702.
20. González-Coma JP, Rodríguez-Fernández J, González-Prelcic N, Castedo L, Heath RW. Channel estimation and hybrid precoding for frequency selective multiuser mmWave MIMO systems. *IEEE J Sel Top Sign Proces*. 2018;12(2):353-367
21. He S, Wang J, Huang Y, Ottersten B, Hong W. Codebook-based hybrid precoding for millimeter wave multiuser systems. *IEEE Trans Signal Process*. 2017;65(20):5289-5304.
22. El Ayach O, Rajagopal S, Abu-Surra S, Pi Z, Heath RW. Spatially sparse precoding in millimeter wave MIMO systems. *IEEE Trans Wirel Commun*. 2014;13(3):1499-1513.

How to cite this article: Smaili N, Djeddou M, Azrar A. Pilot contamination mitigation based on antenna subset transmission for mmWave massive MIMO. *Int J Commun Syst*. 2018;e3768. https://doi.org/10.1002/dac.3768